INTERSTRAND COUPLING AND MAGNETIZATION IN NB₃SN RUTHERFORD CABLES

E. W. Collings and M. D. Sumption,

Laboratories for Applied Superconductivity and Magnetism (LASM), Dept. of Materials Science and Engineering, The Ohio State University, Columbus, OH 43210, U.S.A

Abstract

It is well known by now that interstrand coupling in NbTi Rutherford cables can be suppressed by separating the strand layers with an "insulating" foil or core, typically of stainless steel (SS). Based on the results of an extensive series of studies of NbTi cables with coated strands and cores, the LASM group and its collaborators went on to measure the coupling losses and associated magnetizations of Nb3Sn-wound cables incorporating various kinds of cores and several core widths. In Nb3Sn cables the relatively large product of critical current density and effective strand diameter ($J_c.d_{eff}$) dictates a relatively large low-field persistent current magnetization. The relationship of this to the coupling magnetization at low- and high fields is discussed.

BACKGROUND STUDIES: NB-TI CABLES

Since the pioneering work of Wilson and his colleagues at the then Rutherford Laboratory [1][2] the results of AC conductor research and development have provided a vast literature on eddy-current and coupling loss and its suppression in terms of strand- and conductor design. Cable-level coupling currents have been a recurrent problem in the design of NbTi accelerator magnet cables both as-wound and fully impregnated with resistive solder [3]. Reduced eddy current losses were obtained when a Cu-10Ni barrier was installed around the filamentary bundle within the strand. Lowest coupling losses occur when the strands are individually insulated, the advantage of which is offset by conductor instability. At both Fermilab (FNAL) and at the former SSC Laboratory strand coatings were favored as way of reducing coupling loss.   The influence of coatings on the ramp-rate dependence of loss in Tevatron magnets was discussed by Wake et al. [4]. From just the standpoint of loss full ebonol coating was superior to so-called "zebra coating" (alternate windings of ebonol and stabrite) which in turn was superior to full stabrite coating. Subsequent work addressed the questions of pressure and curing temperature on cable loss. Coupling loss was found to be enhanced if the cables were exposed simultaneously to pressure and heat treatment before measurement [5][6][7]. Taking a cue from these early studies the present authors, now at the Laboratory for Applied Superconductivity and Magnetism (LASM) began a series of investigations into the effect of strand coatings and subsequently cable cores on coupling loss in subsize and full-size Rutherford cables.   Initially such variants in cable design were compared and quantified just in terms of "loss per cycle" of an applied AC field. Later the losses were converted to

crossover and side-by-side "interstrand contact resistances" (ICR), $R_\perp$ and $R_{//}$, respectively, using the following standard network-derived expressions [8] in which $Q_\perp$ represents the "face-on, FO" loss when the applied field is perpendicular to the broad face of the cable and $Q_{//}$ represents the "edge-on, EO" loss

$$Q_\perp = \left(\frac{4}{3}\right)\left(\frac{w}{t}\right)L_p B_m \left[\frac{N^2}{20R_\perp} + \frac{1}{NR_{//}}\right] \cdot \left(\frac{dB}{dt}\right)$$

$$= \left(\frac{2\pi^2}{3}\right)\left(\frac{w}{t}\right)L_p B_m^2 \left[\frac{N^2}{20R_\perp} + \frac{1}{NR_{//}}\right] \cdot f \qquad 1(a)$$

$$Q_{//} = \left(\frac{t}{w}\right)L_p B_m \left[\frac{1}{NR_{//}}\right] \cdot \left(\frac{dB}{dt}\right)$$

where w is the cable width, t the cable thickness, L_p the twist pitch, N the number of strands, and B_m the field sweep amplitude. Moreover one has

$$dQ_\perp / df = \left(\frac{\pi^2}{30}\right)\left(\frac{w}{t}\right)L_p B_m^2 N^2 \left[\frac{1}{R_{\perp,eff.}}\right] \qquad 1(b)$$

LASM's research on coupling loss in cables was stimulated initially by the problems encountered by the SSC's high energy booster (HEB) magnets. Subsequently LASM's interest became coupled to the interests of the large hadron collider (LHC) and high energy particle accelerators in general.   During low energy particle injection and beam accumulation the dipolar field, B, is necessarily small (B_{inj} for the LHC is 0.54 T); then between injection and operation at 8.4 T the dipoles must be ramped at rates, dB/dt, of 7 mT/s. During field ramping the Rutherford cable is the seat of interstrand coupling currents (ISCCs) that loop around a half-pitch of the cable and through the crossover and side-by-side ICRs, $R_\perp$ and $R_{//}$, respectively. Field ramping also generates "supercurrents" [9] or boundary-induced coupling currents (BICCs) [10] that flow over the whole cable length and induce field errors that conform to the period of the twist pitch. BICCs are caused by a dB/dt or by an ICR that varies sharply with distance along the cable, hence the term "boundary". In order to achieve tight control of the particle beam during injection, acceleration, and storage it is necessary to minimize field distortions caused by ISCCs and BICCs [11]. Both of these are suppressed by increasing ICR. But since too high a value reduces cable stability [12] a compromise is

sought. Thus for a standard LHC-type cable $R_\perp$ should be about 15±5 μΩ [11] and $R_{//}$ not less than 0.2 μΩ [10].

We first studied the influence of full strand coating on coupling loss/ICR using a boil-off calorimeter installed at the University of Twente (UoT) [13][14]. The 11-strand test cables had been wound at the Lawrence Berkeley National Laboratory (LBNL) from "SSC-type" strands plated with Ni, Ni+Cr, Cr (2 μm and 5 μm), black Cu oxide, red Cu oxide, electroless Ni-P, and electroless Ni-Fe. Interstrand contact resistances were obtained from the initial slopes of the Q vs. f curves and also more-or-less directly in the LASM's vibrating-sample magnetometer (VSM) using a "diamond-current-simulator" attachment [13]. Using both 11-strand sub-size-cables and LHC-type cables the influences of strand surface condition and coatings, heat treatment (time/temperature) and measurement pressure on ICR was also the subject of detailed study [15]. LASM's initial measurements of LHC-class Rutherford cables with various strand coatings (bare-Cu, Ni, stabrite) and thin ribbon-like cores of various materials (kapton, stainless steel (SS), and Ti) were made magnetically at the Japan National Laboratory for High Energy Physics (KEK) [16] and calorimetrically at UoT. As a result of these experiments the strong supression of coupling loss by the presence of the "insulating" core was clearly demonstrated, $R_\perp$ showing increases of typically two orders of magnitude [14]. By varying the thickness of the core it was possible to study the influence of "internal compaction" on the coupling loss [17][18]. Furthermore the equipment at KEK provided an opportunity to study the influence of "external compaction" i.e. in-cryostat uniaxial pressure (0, 35, and 78 MPa) on the coupling loss [16]. A result of particular interest and importance had to do with the response of stabrite-coated cables to external compaction at 4.2 K. In terms of total loss per cycle (0T-1T-0T) the stabrite cable cured at 170°C responded strongly to pressure. The loss of the uncored cable increased from 3.7 to 20 (10^4J/m^3) in response to an increase in pressure of from 0 to 78 MPa, whereas that of the SS-cored cable remained flat (4.1 to 4.1 x 10^4J/m^3) over that range, see for example Figure 1.

At this stage is it necessary to draw attention to the quantity $R_{\perp,eff}$ defined above in Equations (1). In the standard uncored cable the "face-on, FO," loss, $Q_\perp$, is dominated by coupling currents circulating through the cross-over interstrand contacts of resistance $R_\perp$ whereas in the cored cable measured in an FO field the controlling ICR is the side-by-side value $R_{//}$.

Thus we have chosen to use $R_{\perp,eff}$ (a so-called "effective ICR") as an *index of interstrand coupling strength* when comparing the losses of uncored, partially cored, and fully cored cables.
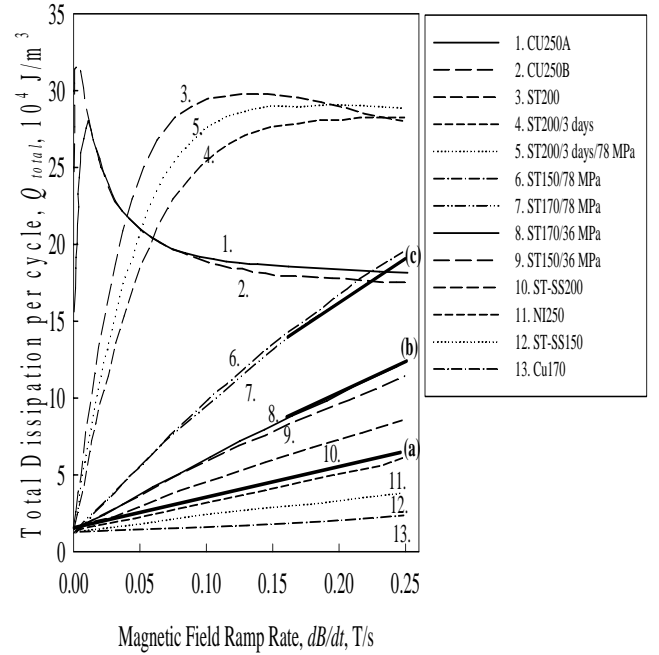

Figure 1: Total loss vs frequency for several cables with coatings and cores. Code "CU" represents bare Cu, "ST" represents stabrite coating, "NI" represents Ni plating, "ST-SS" represents cored stabrite. Line-(a) represents uncored stabrite at 0 Mpa and cored stabrite at all pressures. Lines (b) and (c) represent uncored stabrite at 36 and 78 MPa, respectively [16].

The presence of a stainless steel core strongly suppresses the coupling losses of Rutherford cables wound with *bare-Cu* strand [19][20]. The effective ICR, $R_{\perp,eff}$, of a set of "research-design" cables measured under "pressure release" increased from 5 to 2500 μΩ upon the insertion of a 12.5 μm thick SS core. This impressive result is illustrated in Figure 2 and again in Figure 3 which goes on to show how the ICR of the cored cable decreases with increase in core thickness (12-25-50 μm) as the "internal compaction" increases the strands' side-by-side contact.

In a subsequent series of studies particular attention was given to the properties of standard and cored *stabrite*-coated LHC-type cables. Of particular interest were the effects of

- internal compaction produced by increasing the core thickness at fixed cable thickness [18][21], see Figure 4;
- external compaction by rolling the able to reduced thickness [18][21], see Figure 5;
- varying the width of the stainless steel core [18][21][22].
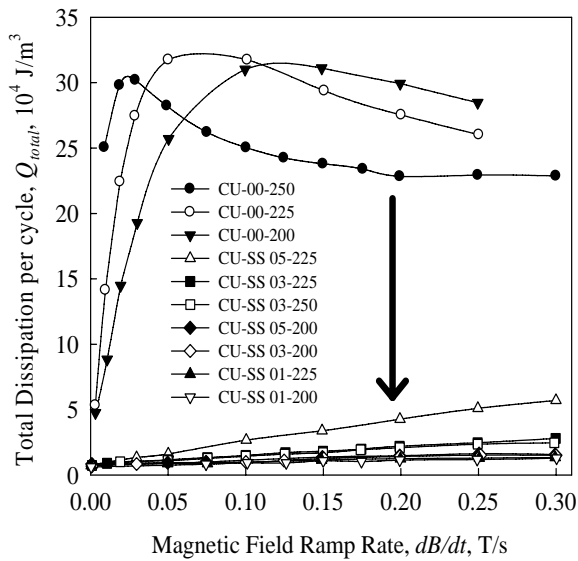
Figure 2: AC losses of bare-Cu cables without a core (upper curves) and after insertion of SS cores of various thicknesses [19].
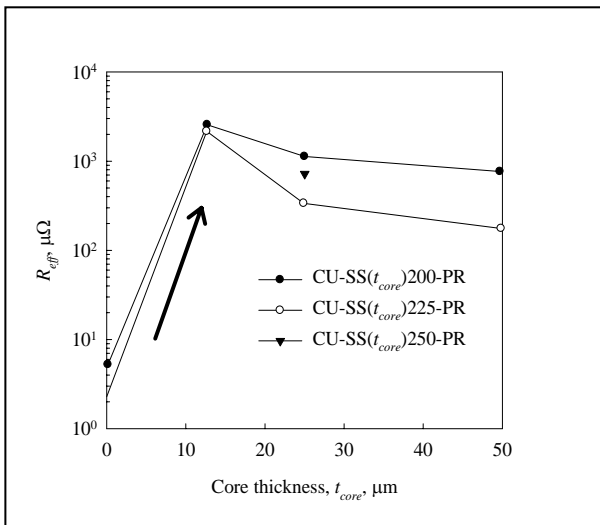

Figure 3: $R_{\perp,eff}$ in response to insertion of cores of thickness 0.5 mil (12.5 μm), 1 mil. (25μm), and 2 mil (50 μm) [20].

Figure 4 illustrates the increase in $R_{\perp,eff}$ that accompanies the insertion of the core (t_{core}, 0 → 25 μm) followed by a small decrease as increasing core thickness improves the side-by-side contact (cf. Figure 3).

In Figure 5 we start of with a cored cable and apply gradually increasing levels of external compaction. The 170°C-cured cable experiences a rapid decrease in $R_{\perp,eff}$ again due to improving side-by-side contact; not so for the cable cured at 200°C whose strands are well sintered.

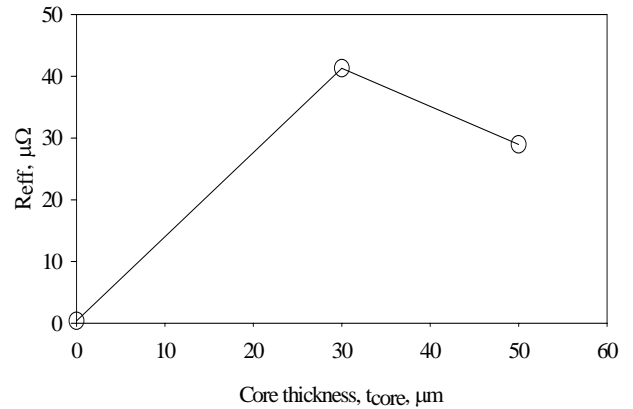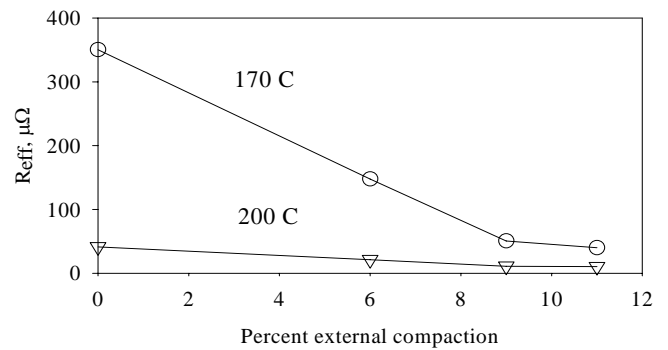Figure 4: $R_{\perp,eff}$ vs. core thickness, t_{core}, for stabrite-coated cables cured at 200°C [18].

Figure 5: $R_{\perp,eff}$ vs. percent external compaction for stabrite-coated cables cured at 170°C and 200°C [18].

The effect on per-cycle loss, Q_{total} of varying the core width is illustrated in Figure 6 for 28-strand stabrite cables 15 mm wide wound with cores of width $w_{core} = 0$, 3.2, 6.4, 9.5. and 12.7 mm, corresponding to about 0%, 20%, 50%, 75% and 100% of the available cable width. Figure 7 presents the cable-loss data in terms of $R_{\perp,eff}$. The figure shows that the goal of 15 μΩ would be achieved at a core width of 8.5 mm or 67% of $w_{core,max}$. Shown for comparison in the figure (at position "CN") is the measured $R_{\perp,eff}$ of an uncored stabrite cable that had received the CERN-recommended heat treatment of 8h/200°C in air. At 26.7 μΩ its $R_{\perp,eff}$ is equivalent to that of a cable with a core of width ~68% of w_{max}.
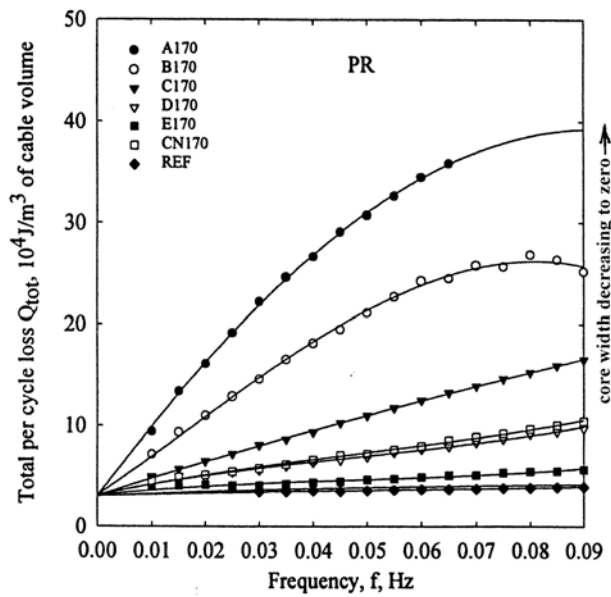
Figure 6: Loss vs. frequency for a series of cored stabrite cables with cores of widths 0, 3.2, 6.4, 9.5, and 12.7 mm (full) cured at 170°C. Included is a result for an uncored "CERN-processed" stabrite cable, CN170, cured at 200°C, see [18],[21] and [22].
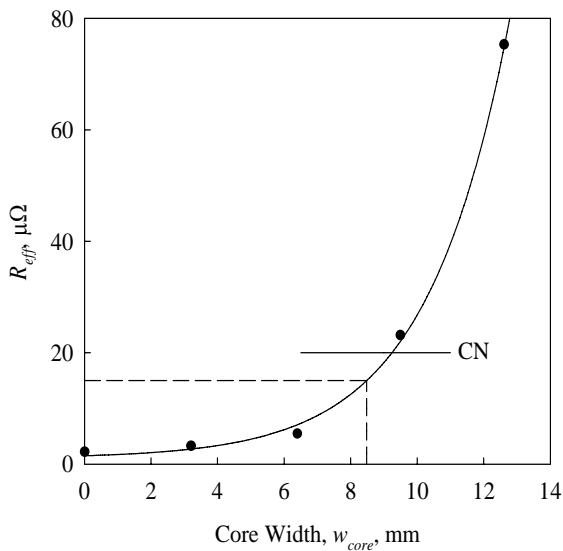

Figure 7: $R_{\perp,eff}$ vs.core width for the cables of Figure 6

These NbTi-cable-based studies of strand coatings, preparation heat-treatment conditions, the effects of internal and external compaction, coupling loss suppression by the introduction of cores, and the effects of varying the core width, provided the background for extensive research into the properties of standard- and specially prepared Nb$_3$Sn cables.

COUPLING LOSS, ICR AND MAGNETIZATION IN NB$_3$SN CABLES

Coupling loss and ICR

Some AC loss results for a set of Nb$_3$Sn cables in the face-on (FO) and edge-on (EO) orientations are depicted in Figure 8. In many cases the coupling loss is so high that $R_{\perp,eff}$ can no longer be derived from a linear Q vs f slope, Equation (1b), as was generally the case for NbTi cables. Instead, the so-called "critical-frequency" approach must be used.
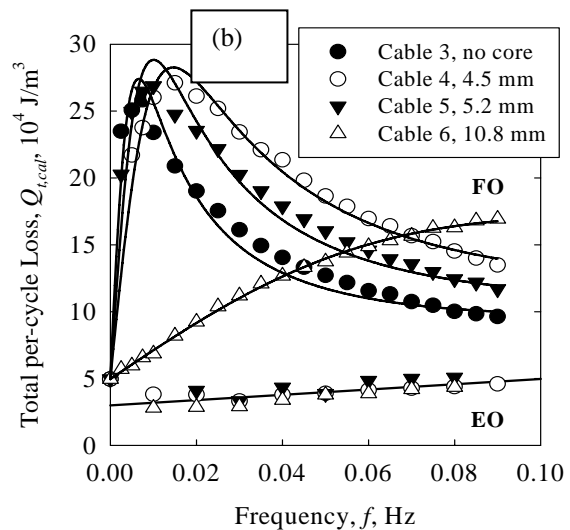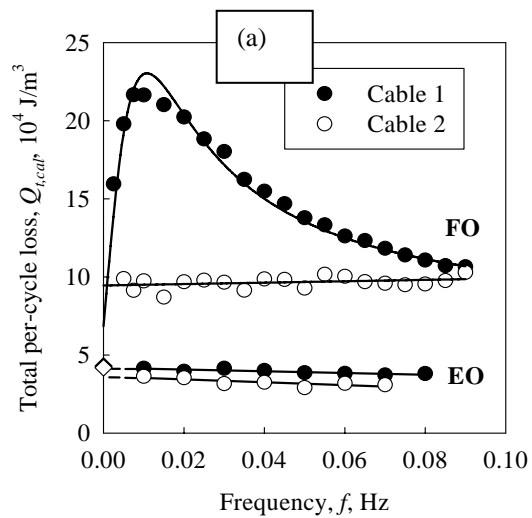

Figure 8: (a) AC losses for an un-cored Nb$_3$Sn cable (filled circle) compared with those for a full-cored cable [33]. (b) AC losses for un-cored (filled circle) and variously cored Nb$_3$Sn cables. Even the 10.0 mm core is in this case only partially effective, cf. (a) [32].

The simultaneous generation and decay of coupling currents gives rise to a maximum in Q (f) at a critical

frequency $f_c = 1/2\pi\tau_c$ (where τ_c is the corresponding relaxation time) following the general relationship:

$$Q(f) = Q_0 \frac{f/f_c}{1+(f/f_c)^2} \qquad (2)$$

This applies to strand eddy currents as well as cable- and cable-stack coupling currents with relaxation times of τ_{cab} and τ_{stack}, respectively. Relationships between the individual-cable relaxation time τ_{cab} and the relaxation time of the stack τ_{stack} lead to f_c– based ICR values designated $R_{\perp,fc}$. According to Verweij [10]:

$$R_{\perp,fc} = 2\pi(DE)f_c \qquad (3)$$

which is obtained by combining $\tau_{cab}R_\perp = D$ (where D is a function of the individual-cable properties, N and L_p, see Equation (1)) with $\tau_{stack} / \tau_{cab} = 1/(2\pi f_c \tau_{cab}) = E$ (where E is a function of w/t and N_C, the number of cables in the stack). Typical Q vs f curves following the Equation (2) prescription are depicted in Figures 9 and 10.
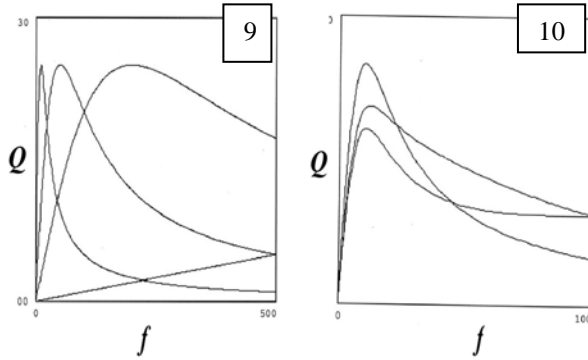

Figure 9: Loss vs. frequency. Each cable has a single homogeneous ICR, each given by its initial slope dQ/df and/or its critical frequency, f_c – cf. Figure 2.

Figure 10: Loss vs. frequency. Each cable exhibits a blend of two ICRs, one common to all cables and the other different for each cable. Thus each curve possesses a second f_c that elevates its tail, see [30].

In collaboration with LBNL and the Fermi National Accelerator Laboratory (FNAL) an extensive series of specially wound and treated Nb₃Sn cables were prepared for AC-loss measurement at UoT. Particular attention was paid to the following issues:

- ICR in response to the introduction of a core and to variation of core design;
- Cable designs for improved stability;
- ICR in response to variation of cable pre-heat-treatment (surface) condition and to variation of final heat-treatment conditions;
- ICR in response to variation of core width;
- the cables' so-called "hysteretic loss" or persistent current magnetization based on the properties of the component strands.

Introduction of the core and variation of core design

Over a period of several decades numerous groups have modified the ICR of NbTi cables by applying metallic or insulating coatings to the strands either before or after cabling. Strands have been coated with Cr, Ni, NiCr, SnNi, Zn, ZnNi, CuO, NiP, or dip-coated SnAg (stabrite). In comparison to NbTi/Cu the severity of Nb₃Sn's RHT (Reaction Heat Treatment) leaves only a few options open for pre-RHT surface treatment. In fact only two surface treatments have received practical consideration: Cr plating and carbon deposition from a synthetic oil coating decomposed during RHT. Our group believes that the most effective and reproducible way of controlling the ICR of a Nb₃Sn Rutherford cable is through the introduction of an SS core. As demonstrated in [23] the presence of a full width thin SS core can result in a substantial increase in $R_{\perp,eff}$ e.g from 1.8 to 70 μΩ. The latter value is arguably too high to ensure stability, for which reason reduced-width cores were recommended, see below. The ICR of a Nb₃Sn cable can also be altered through changes in the actual strand architecture which moderates the current flow across the contacts between crossing strands [24]. An interesting core arrangement implemented by LBNL consisted of a double core: two strips of bimetallic Cu/SS sandwiched together with the SS surfaces (with their attached native oxide layer) facing each other [25]. The idea was to inhibit cross-over contact in the usual way while at the same time improving side-by-side contact (hence current sharing and stability) by allowing the Cu surfaces to sinter to the strands.

Cable designs for improved stability

Additional Cu included in the internal structure of the cable was intended to contribute stability. Of course the Cu can also be attached to the outside of the cable either as a pair of strips placed on the outside surfaces, or as a continuous strip helically wound along the outside of the cable. The purpose of the added Cu, which is intended to diffusion bond to the strands during RHT, is to improve stability and provide passive quench protection. Although we were not set up to measure those quantities, AC loss experiments were performed on cored cables to explore whether the Cu was added at the expense of coupling loss. It turned out that the added Cu was beneficial; in the test sample studied $R_{\perp,eff}$ was lowered from an immeasurable high value (not unexpected for a resistive-core cable) into the range of 30-60 μΩ.

ICR dependence on heat treatment

As stated above, many different surface coating have been applied to NbTi strand in order to control the properties of the cable wound from them. But the severity of Nb₃Sn's RHT leaves only a few options open for pre-RHT surface treatment, e.g. Cr plating and the application or retention of lubricating oil which subsequently decomposes to C during RHT. Since the effects of applied surface coatings

had been well researched it was decided, in a collaboration with LBNL, to examine the influences of various pre-RHT cable-cleaning procedures (acetone rinsing, HCl rinsing) on the ICR of uncored cables. Although the ICRs were mostly in the range of 0.2 – 1.6 $\mu\Omega$, one of the clean uncored cables produced an ICR of 13±2 $\mu\Omega$. The results are evidently so unpredictable that one or other of the above contact-controlling techniques is recommended.

In a companion series of studies, this time in collaboration with FNAL, we explored the influence of preparation conditions (insulation, RHT, and impregnation schedules) on the ICRs of uncored cables as determined at UoT using both calorimetric and magnetic techniques. All cables measured exhibited a principal $R_{\perp,eff}$ of 0.4 $\mu\Omega$ although one of the cables exhibited a secondary $R_{\perp,eff}$ of 4 $\mu\Omega$. It turned out that these experiments provided the first quantitative evidence for $R_{\perp,eff}$ variability in Nb_3Sn cables, one that could be resolved into two distinct $R_{\perp,eff}$s. Such $R_{\perp,eff}$ anisotropy or inhomogeneity would be favored by the severe turks-heading which, applied to the cable during its final stage of formation, results in a pronounced flattening of the strands along its edges, thereby setting the stage for the development of uneven interstrand contact during further compaction and heat treatment. Further aspects of cable inhomogeneity are discussed in [30]

ICR dependence on core width

Calorimetric and magnetic measurements were made at UoT on a series of 14-mm-wide Rutherford cables wound at FNAL with cores of widths 4.5, 5.2, and 10.8 mm. The resulting FO-measured $R_{\perp,eff}$s were compared with that of the uncored cable whose uncored $R_{\perp,eff}$ of 0.19 $\mu\Omega$ conformed well to the results of several previous measurements e.g. 0.16-0.4 $\mu\Omega$. On the other hand, the cored results were much lower than expectation; and unlike those of the earlier measurements these $R_{\perp,eff}$s did not increase monotonically with core width, cf. Figure 7.

Furthermore the intended full-width core yielded an $R_{\perp,eff}$ of only 8 $\mu\Omega$, i.e., very much lower than the expected 50-100 $\mu\Omega$ for a full-width core. The explanation has to do with the locations and effective widths of the cores both of which were studied using scanning electron microscopy (SEM). Undulation of the core's cross-section as it follows the curves of the nested strands causes it to shrink below its nominal width such that the widest core was not only less than full width (covering only 77% of the 12.2 mm (I.D.) available cable width) but also off-center. We estimate based on Figure 7 and reference [21] that a coverage increase of from 75% to 100% could result in a four-fold increase in $R_{\perp,eff}$ which in this case could raise $R_{\perp,eff}$ to about 32 $\mu\Omega$. An even greater increase would accompany the shift of the core to the center of the cable and bring its $R_{\perp,eff}$ more into line with previously measured values [24][25].

ICR of cored and un-cored Nb_3Sn Rutherford cables

We conclude this discussion of core effects with a tabulation of the collected results of our ICR measure-ments on cored and uncored Nb_3Sn Rutherford cables. Due to interstrand sintering the uncored ICRs are generally very small – mostly around 0.3 $\mu\Omega$ according to Table 1. A full width core may raise the ICR into the 25-50 $\mu\Omega$ range although some very high values (200 $\mu\Omega$ and immeasurably large, "∞") have been obtained. Narrow and/or misplaced cores are not very effective in reducing coupling loss.

Table 1: Nb_3Sn Cables -- Collected Effective- ICR Results, $R_{\perp,eff}$, $\mu\Omega$

NO CORE	Full-width core	Ref.
<0.1 (0T), 2.7 (1T)	33 (0T), 78 (1T)	[24]
0.24	23	[25]
	24	"
	53	"
	"∞"	"
0.15 (0T), 0.4 (1T)		[28][29]
13.0 (0T), 11.5 (1T)		"
1.47 (0T), 3.09 (1T)		"
0.33 (0T), 1.27 (1T)		"
0.30 (0T)		"
0.4, 4		[30]
0.19, 0.21	8	[31][32]
0.31	209	[33]

HYSTERETIC OR PERSISTENT CURRENT MAGNETIZATION OF NB3SN CABLES

Magnetization near injection

Underlying both field quality and flux-jump stability, strand- and hence cable magnetization may be considered to be a "critical defining parameter" in precision dipole applications [34]. As deduced in [34] the persistent current shielding-magnetization of a NbTi LHC-type cable at injection, $M_{sh.inj.cable}$(1.9K,0.54T) is estimated to be about 4.9 kA/m. We show this to be commensurate with the cable's coupling-current magnetization during the injection ramp, $M_{coup(ramp)}$. Starting with Equation (1a) and recognizing that in general $Q_\perp = 4M_{coup}B_m$ we find:

$$M_{coup} = \left(\frac{1}{3}\right)\left(\frac{w}{t}\right)L_p\left(\frac{dB}{dt}\right)\left[\frac{N^2}{20R_{\perp,eff}}\right] \qquad (4)$$

We next insert a set of typical cable parameters, such as a width w of 15 mm, a thickness t of 1.78 mm (giving a ratio w/t=7.99), L_p=55.1 mm, N=28 strands and a dB/dT of 7 mT/s, we obtain

$$M_{coup(ramp)} = \frac{4.03x10^4}{R_{\perp,eff}(\mu\Omega)} \text{ A/m} \quad (J/m^3T) \qquad (5)$$

After inserting the LHC-recommended value $R_{\perp,eff} = 15$ $\mu\Omega$ we find $M_{coup(ramp)} = 2.69$ kA/m. Both this and $M_{sh.inj.cable}$ are easily corrected electromagnetically. Not so for Nb$_3$Sn Rutherford cables whose hysteretic magnetizations, based on VSM measurements on strands to ±400 mT [33] have been shown to be about $3x10^5$ J/m^{3}T (300 kA/m) two orders of magnitude higher, Figure 11.

In simple un-cored cables the quantity $R_{\perp,eff}$ defined in Equations (1a) and (1b) is a true interstrand contact resistance. But in association with Equation (4), and Equation (5) as a special case, it becomes an index of coupling magnetization. Furthermore, magnetization in general can be usefully parameterized in terms of $R_{\perp,eff}$. With this in mind we repeat, in principle, the low-field cable-magnetization calculation, previously based on NbTi J_c data [34], this time for a Nb$_3$Sn cable at 4.2 K assuming (i) a Kramer-extrapolated $J_{c,non-Cu,0.5T} = 16.8$ x $J_{c,non-Cu,12T}$, (ii) a strand fill-factor of 0.5, (iii) a cable packing factor of 0.9, such that $J_{c,cab,0.5T} = 0.5$ x 0.9 x 16.8 x $J_{c,non-Cu,12T} = 7.56\ J_{c,non-Cu,12T}$. It follows that:

$$M_{cab,0.5T}(A/m) = \left(\frac{2}{3\pi}\right)J_{c,cab,0.5T}(A/m^2)\times d_{eff}(m)$$

$$= 1.60\times J_{c,non-Cu,12T}(A/mm^2)\times d_{eff}(\mu m) \qquad (6)$$

Magnetic Field, μ_0H, mT

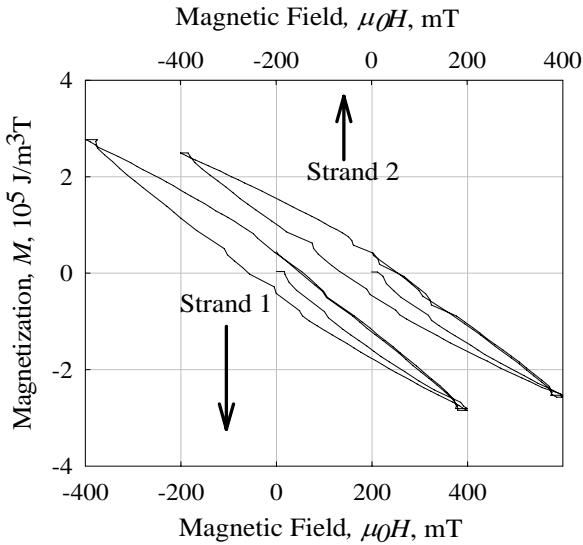Figure 11: VSM-measured hysteresis loops for a pair of Nb$_3$Sn extracted strands for "un-penetrated" field-sweep amplitudes of ±400 mT [33].
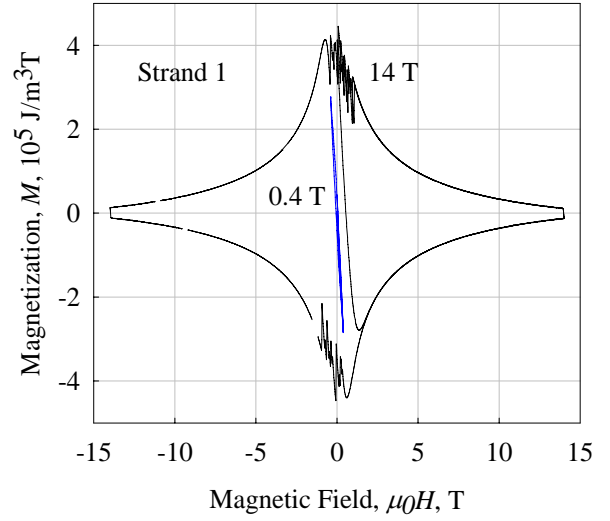
Figure 12: VSM-measured hysteresis loops for a Nb$_3$Sn extracted strand at field-sweep amplitudes of ±400 mT and ±14 T [33].

with $J_{c,non-Cu,12T} = 3000$ A/mm^2 as for a good quality HEP strand, and a typically measured d_{eff} of ~80 μm $M_{cab,0.5T} = 3.84x10^5$ A/m and the corresponding individual-strand magnetization would be $4.27x10^5$ A/m. This is in good agreement with the fully penetrated magnetization data of Figure 12, and again two orders of magnitude greater than the NbTi values.

We next couple together Equations (5) and (6) in order to obtain an explicit expression for $R_{\perp,eff}$ in the injection region, demonstrating its use as a "magnetization parameter". The result is:

$$R_{\perp,eff}(\mu\Omega) = \frac{2.5\times10^4}{J_{c,non-Cu,12T}\times d_{eff}} \qquad (7)$$

with J_c in A/mm^2 and d_{eff} in μm

Equation (7) plotted in Figure 13 shows that the use of Nb$_3$Sn strand leads to $R_{\perp,eff}$s that are mostly below 0.3 μΩ, which from a magnetization standpoint seems to negate the purpose of introducing a core.

Cable magnetization at higher fields

The above analyses emphasize the unsuitability of Nb$_3$Sn cable for low field precision-field operation. Its high persistent current magnetization degrades quality, Equation (5), and produces flux jumping, Figure 12. The situation improves rapidly as the magnet's operating point moves towards higher fields for two reasons: (1) In moving from 0.5 T to 12 T, for example, the strand's $J_c(H)$ decreases by a factor 16.8 (based on the above mentioned Kramer factor) or 18.3 according to Figure 12. (2) The transport current needed to generate the field reduces the strand's magnetization by a factor $(1-i^2)$, e.g. [35]. Assuming a high-field i of 0.8 the combined magnetization-reduction factor would be 1/49. This

would raise the $R_{\perp,eff}$ of, for example, a d_{eff} = 30 μm 2.5 kA/mm² strand from 0.32 μΩ (point **x** in Figure 13) to an acceptable 15 μΩ.
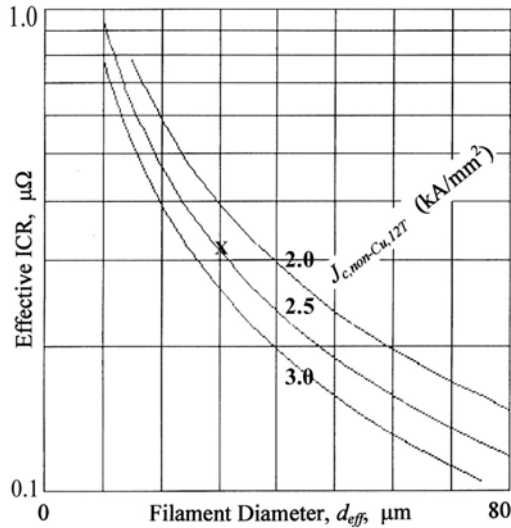

Figure 13: "Effective ICR", regarded as a magnetization parameter, plotted as function of d_{eff} for three values of $J_{c,non-Cu,12T}$ (kA/mm²)

CONCLUSIONS

- NbTi-cable studies pointed the way by showing how:
  - The introduction of a full-width SS core strongly suppresses coupling loss and the crossover ICR , $R_{\perp}$ (and its "effective" value, $R_{\perp,eff}$).
  - The core-suppressed $R_{\perp,eff}$ could be tuned by vary the width of the core.
- The above ideas were transferred into the Nb₃Sn cable program wherein it was again shown that strong loss suppression and increased ICR would accompany the introduction of SS cores and composite cores of SS and Cu.
- In experiments on a set of Nb₃Sn cables with cores of various widths it was found that:
  - ICR varied rapidly with core width;
  - Narrow cores produced little loss suppression;
  - The level of suppression was sensitive to the position of the core indicating that care is needed to ensure that the core is well centered.
- The EO loss tended to be frequency independent and hence attributable to the "hysteretic" persistent-current magnetization of the strands.
- Under LHC injection conditions, B_{inj} = 540 mT and $(dB/dt)_{inj}$ = 7 mT/s, strand magnetization also dominates the FO magnetization of the Nb₃Sn cable. As a result of excessive magnetization and the

associated flux jumping the Nb₃Sn Rutherford cable is unsuitable for low-field operation.
- Away from injection, and in operating fields of 12 T or more, the cable magnetization drops by a factor of at least 49 into an acceptable range of values.

REFERENCES

[1] M.N. Wilson, C.R. Walters, J.D. Levin, et al., *J. Phys. D: Appl. Phys.* **3** 1517-1583 (1970)
[2] G.H. Morgan, *J. Appl. Phys.* **44** 3319-3322 (1973)
[3] J.A. Eikelboom and J.A. Roeterdink, *IEEE Trans. Magn.* **24** 1463-1466 (1988)
[4] W. Wake, D. Gross, R. Yamada, et al., *IEEE Trans. Magn.* **15** 141-142 (1979)
[5] Y.Z. Lei, T. Shintomi, A. Terashima, et al., *IEEE Trans. Appl. Supercond.* **3** 747-750 (1993)
[6] A. Kimura, N. Kimura, Y. Makida, et al., *IEEE Trans. Magn.* **30** 2515-2518 (1994)
[7] G.T. Mallick, Jr., D. Natelson, W. J. Carr, Jr., et al., *IEEE Trans. Appl. Supercond.* **3** 744-746 (1993)
[8] V.E. Sytnikov, G.G. Svalov, S.G. Akopov, et al., *Cryogenics* **29** 929-930 (1989); see also V.E. Sytnikov, and I.B. Peshkov, *Adv. Cryo. Eng. (Materials)* **40** 537-542 (1994)
[9] L. Krempasky and C. Schmidt, *Physica C* **310** 327-334 (1998)
[10] A.P Verweij, *Ph.D. Thesis*, University of Twente Press, 1995
[11] Z. Ang, I. Bejar, D. Richter, et al., *IEEE Trans. Appl. Supercond.* **9** 735-741 (1999)
[12] A.K. Ghosh, W.B. Sampson, S.W. Kim, et al., *Physica C* **310** 335-339 (1998)

[13] M.D. Sumption, H.H.J. Ten Kate, R.M. Scanlan, et al*., IEEE Trans. Appl. Supercond.* **5** 692-696 (1995)

[14] M.D. Sumption, R.M. Scanlan, A. Nijhuis, et al., *Adv. Cryo. Eng. (Materials)* **42** 1303-1311 (1997)

[15]   M.D. Sumption, E.W. Collings, R.M. Scanlan, et al., *Cryogenics* **39** 197-208 (1999)

[16] E.W. Collings, M.D. Sumption, R.M. Scanlan, et al., *Adv. Cryo. Eng. (Materials)* **42** 1225-1232 (1997)

[17] E.W. Collings, M.D. Sumption, S.W. Kim, et al., *IEEE Trans. Appl. Supercond.* **7** 962-966 (1997)

[18] M.D. Sumption, R.M. Scanlan, and E.W. Collings, *IEEE Trans. Appl. Supercond.* **11** 2571-2574 (2001)

[19] E.W. Collings, M.D. Sumption, S.W. Kim, et al*., Proc. 16th ICEC/ICMC Conference*, ed. By T. Haruyama,
        T. Mitsui, K. Yamafuji (1996)

[20] M.D. Sumption, E.W. Collings, R.M. Scanlan, et al., *Supercond. Sci. Tech.* **14** 888-897 (2001)

[21] M.D. Sumption, E.W. Collings, R.M. Scanlan, et al., *Cryogenics* **41** 733-744 (2001)

[22] M.D. Sumption, E.W. Collings, A. Nijhuis, et al., *Adv. Cryo. Eng. (Materials)* **46** 1043-1049 (2000)

[23] M.D. Sumption, E.W. Collings, R.M. Scanlan, et al., *Adv. Cryo. Eng. (Materials)* **44** 1077-1084 (1998)

[24] M.D. Sumption, E.W. Collings, R.M. Scanlan, et al., *Cryogenics* **39** 1-12 (1999)

[25]   M.D. Sumption, R.M. Scanlan, Yu.A. Ilyin, et al., *Adv. Cryo. Eng. (Materials)* **50** 781-788 (2004)

[26] E.W. Collings, M.D. Sumption, R.M. Scanlan, et al., *Adv. Cryo. Eng. (Materials)* **48** 1153-1160 (2002)

[27] M.D. Sumption, E.W. Collings, R.M. Scanlan, et al., *IEEE Trans. Appl. Supercond.* **13** 2376-2379 (2003)

[28] E.W. Collings, M.D. Sumption, D.R. Dietderich, et al., *Adv. Cryo. Eng. (Materials)* **52** 851-858 (2006)

[29] E.W. Collings, M.D. Sumption, D.R. Dietderich, et al., *IEEE Trans. Appl. Supercond.* **16** 1200-1203 (2006)

[30] E.W. Collings, M.D. Sumption, G. Ambosio, et al., *IEEE Trans. Appl. Supercond.* **17** 2494-2495 (2007)

[31] E.W. Collings, M.D. Sumption, E. Barzi, et al., *Adv. Cryo. Eng. (Materials)* **54** 285-292 (2008)

[32] E.W. Collings, M.D. Sumption, E. Barzi, et al., *IEEE Trans. Appl. Supercond.* **18** 1370-1373 (2008)

[33] E.W. Collings, M.D. Sumption, M.A. Susner, et al., *IEEE Trans. Appl. Supercond.* **18** 1301-1304 (2008)

[34] E.W. Collings, M.D. Sumption, and E. Lee, *IEEE Trans. Appl. Supercond.* **11** 2567-2570 (2001)

[35] M.A.R. LeBlanc, *Phys. Rev. Lett.* **11** 149-152 (1963)